

The influence of secondary ion beam irradiation on the formation of Si nanocrystals during dual ion beam sputtering

Jae Kwon Kim, Kyu Man Cha, Jung Hyun Kang, Yong Kim*, Jae-Yel Yi, Tae Hun Chung, Hong Jun Bark

Department of Physics, Dong-A University, Hadan-2-dong, Sahagu, Pusan 604-714, South Korea

Received 18 February 2004; received in revised form 15 October 2004; accepted 19 October 2004

Available online 23 November 2004

Abstract

We investigate the deposition of SiO_x films by dual ion beam sputtering system with emphasis on secondary ion beam irradiation effect. We observe the intense photoluminescence (PL) from SiO_x samples with apparent oxygen contents, x_{app} , in the narrow range of $1.1 \leq x_{\text{app}} \leq 1.4$, after post-deposition annealing at 1100 °C. This indicates the formation of Si nanocrystals as evidenced by cross-sectional transmission electron microscope (TEM) image. Ar ion beam irradiation changes PL peak positions in ion-beam exposed region. This effect is utilized for achieving the area-selective formation of Si nanocrystals by inserting a shadow mask in secondary ion beam during deposition.

© 2004 Elsevier B.V. All rights reserved.

PACS: 61.46.+w; 73.40.Qv; 81.65.Mq; 68.55Jk

Keywords: Nanostructures; Ion bombardment; Sputtering; Luminescence

1. Introduction

Since the first discovery of the light emission from porous silicon [1], the interest toward Si-based optoelectronics has rapidly increased. Due to the better compatibility with standard ultra-large scale integrated circuit (ULSI) processes, Si nanocrystals in a dielectric matrix have gained much interest. The standard approach for the formation of Si nanocrystals is the utilization of the prolonged annealing of SiO_x ($x < 2$) films at temperatures higher than 900 °C. During the annealing, phase separation and precipitation take place owing to the energetic stability of Si and SiO_2 phases. The various attempts for the deposition of SiO_x films include ion-implantation [2], chemical vapor deposition (CVD) [3–6], reactive evaporation [7], co-sputtering [8], and ion beam sputtering [9], etc.

SiO_x films yield highly luminescent nanocrystals with large density regardless of deposition methods. The previous methods are not area-selective and thereby nanocrystals are precipitated in whole deposited area. However, the area-selective technique for Si nanocrystals formation may offer a processing flexibility in future ULSI processes with nanocrystal light emitting devices.

Weissmantel [10] has first used the dual ion beam sputtering (DIBS) for reactive compound deposition. Harper et al. [11] have extensively investigated about the application aspects of DIBS. DIBS system usually comprises two ion beam sources. Primary source serves as a sputtering ion source and the other ion source is utilized as a secondary ion source. Secondary ions could be utilized for several purposes. The first one is for the pre-cleaning of surface before deposition is initiated. The second one is for the surface activation by ion irradiation during deposition. The secondary ion beam has been utilized to significantly enhance and control the film properties. The effect of secondary ion beam irradiation is the densification of film

* Corresponding author. Tel.: +82 512007276; fax: +82 512007232.

E-mail address: yongkim@daunet.donga.ac.kr (Y. Kim).

and the reduction of film stress. This is due to the fact that secondary ions preferentially sputter deposits and contaminants with lower bonding energies than that of constituent material [12].

Recently Lambrinos et al. [13] investigated the electrical properties of SiO_2 , SiO_xN_y , and SiN_x films deposited by DIBS. Reactive assist ions of N_2 have been used instead of inert ions. Ray et al. [14] have observed the modification of refractive indices of films by varying secondary ion energy during SiO_xN_y deposition. The possibility for the area-selective control of film properties has been shown by Weissmantel [10]. By shadowing a region of substrate from nitrogen ion beam, area-selective modification of film property has been achieved.

In this paper, we employ a similar idea but extend to the area-selective formation technique of Si nanocrystals by using ion beam irradiation during DIBS.

2. Experimental details

SiO_x films were deposited by employing a DIBS system. DIBS system consists of two Kaufman-type broad-beam ion sources. Ultra-pure (99.999%) Ar gas was supplied to both ion sources. Fig. 1 shows a schematic illustration of our DIBS system. Primary ion source of 2.5 cm diameter with the incident angle of 65° served as a sputtering ion source. P-type (100) silicon wafer (resistivity $\sim 10 \Omega \text{ cm}$) was used as a sputtering target. The beam energy and beam current of the primary ion source were 750 eV and 7 mA, respectively. A secondary ion source of 6 cm diameter with the incident angle of 37° was used. The beam current of the secondary ion source was 10 mA and beam energy was a variable parameter (0–200 eV). O_2 gas (99.999%) diluted to 10 vol.% in Ar was introduced into the deposition chamber for

a reactive deposition. The operating pressure was kept at $8 \times 10^{-2} \text{ Pa}$ by adjusting the flow of Ar while the partial pressure of O_2 gas was varied. No intentional heating was applied on substrate during deposition. SiO_x films were deposited for 2–4 h on 3-in. p-type (100) Si wafer (resistivity $\sim 10 \Omega \text{ cm}$) after standard cleaning sequence to remove organic and inorganic surface contaminants.

Deposited SiO_x films were subsequently annealed at 1100°C for 2 h in N_2 atmosphere. They were further annealed at 450°C for 3 h in a forming gas (N_2 90%, H_2 10%) for H_2 passivation. Photoluminescence (PL) was excited by 488 nm Ar^+ ion laser (30 mW and $\sim 1 \text{ mm}$ beam diameter) mechanically chopped at a frequency of 500 Hz. PL spectra were measured using a 0.5 m monochromator (Dongwoo optron DM500). The PL signal was detected by a photomultiplier tube (Hamamatsu R928) by using standard lock-in technique (Stanford research SR810). Monochromator was calibrated in the regions from 500 to 900 nm using a tungsten–halogen lamp. All measurements were done at room temperature. The cross-sectional transmission electron microscope (TEM) image was observed by using a JEOL JEM-2010 equipment through the preparation technique including mechanical polishing and Ar ion milling at 4.5 KV in a Gatan DuoMill 660 DIF. The bonding configurations in oxide matrix were measured by a Fourier transform infrared spectroscopy (FTIR, Biorad Excalibur FTS-3000). According to Pai et al. [15], Si–O–Si stretching vibration frequency shifts linearly with the oxygen content, x provided that the film is homogeneous. Pai et al. are dealing with plasma enhanced CVD films, meaning that there is a substantial hydrogen content. In contrast, during the secondary ion beam irradiation some Ar atoms would be incorporated in our films. In addition, the level of stresses in films deposited by these two techniques is not the same. All these factors may lead to the shift of Si–O–Si stretching peak. However, it may be useful to define apparent oxygen content, x_{app} in SiO_x film determined from the position of the Si–O–Si stretching vibration frequency, ν (cm^{-1}) using the same equation proposed by Pai et al. as shown below;

$$x_{\text{app}} = (0.02 \times \nu) - 19.3. \quad (1)$$

3. Results and discussion

First, we grow several SiO_x films ($0.56 \leq x_{\text{app}} \leq 1.6$) with various apparent oxygen content by adjusting O_2 partial pressure, $P(\text{O}_2)$, from 0.8×10^{-3} to $2.1 \times 10^{-3} \text{ Pa}$. In this case, secondary ion source is not activated. Fig. 2 shows the FTIR spectra of SiO_x films with various $P(\text{O}_2)$. The IR band found at around 1050–1080 is attributed to Si–O–Si stretching vibration [15]. Si–O–Si stretching vibration frequency systematically shifts toward higher frequency as increasing $P(\text{O}_2)$. In addition, the narrowing of the width of Si–O–Si stretching vibration is found indicating the reduced randomness of Si–O bonding configurations.

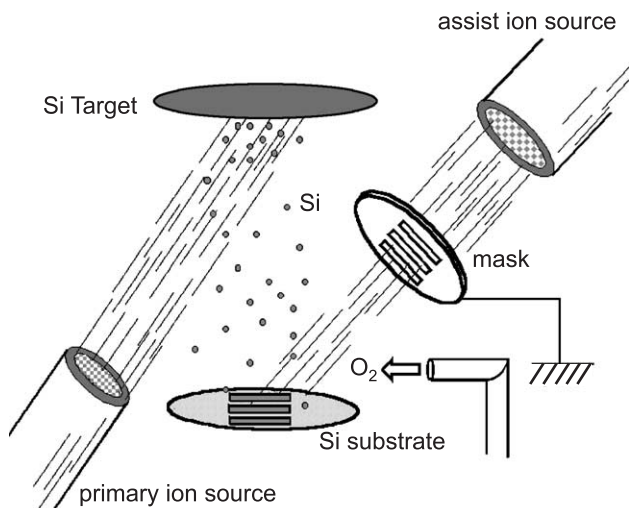


Fig. 1. Schematic illustration of dual ion beam deposition with a grounded shadow mask.

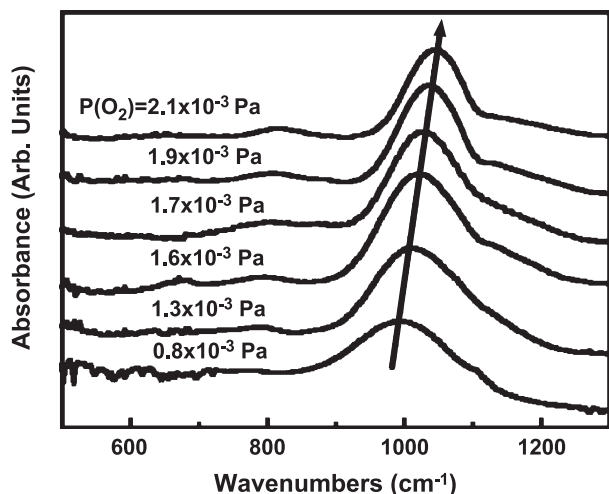


Fig. 2. Infrared spectra of SiO_x films with various O_2 partial pressures during deposition. The spectra are shifted for clarity. The arrow indicates the variation of Si–O–Si stretching vibration.

Then we activate secondary ion beam. Fig. 3 show the FTIR spectra of SiO_x films with 1.9×10^{-3} Pa of $P(\text{O}_2)$ by varying the energies of secondary Ar ions. Si–O–Si stretching vibration frequency systematically shifts toward higher frequency as increasing the energy of assist ions. Fig. 4 show the figures for summarizing the variations of apparent oxygen content, x_{app} as functions of $P(\text{O}_2)$ and assist ion energy, respectively. From Fig. 4(a), the apparent oxygen content is linearly proportional to $P(\text{O}_2)$. Therefore DIBS technique is quite reliable in preparing SiO_x films with desired oxygen content. In addition, the linear relationship means that x_{app} adopted from Pai's relation is a good indication parameter for reflecting oxygen content variation in films.

Fig. 4(b) shows the superlinear increase of x_{app} with ion beam energy and the film grown under 200 eV ion beam

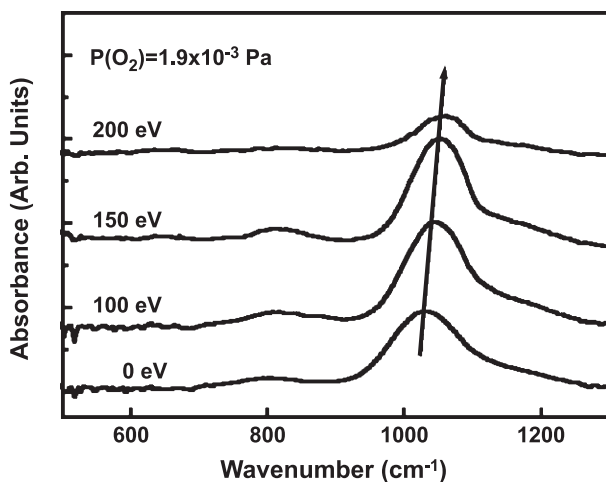


Fig. 3. Infrared spectra of SiO_x films irradiated with secondary ions of various ion beam energies. O_2 partial pressure is 1.9×10^{-3} Pa during deposition. The spectra are shifted for clarity. The arrow indicates the variation of Si–O–Si stretching vibration with assist ion beam energy.

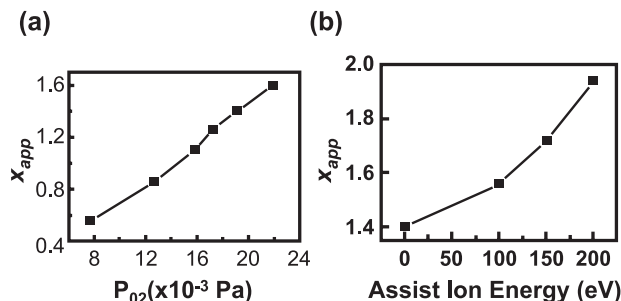


Fig. 4. (a) the variation of x_{app} as a function of oxygen partial pressure and (b) the variation of x_{app} as a function of assist ion beam energy.

irradiation is almost close to stoichiometric SiO_2 film. Microstructure of SiO_x films has been discussed either by random mixture model [16] or random bond model [17]. As discussed by Lombardo et al. [4] from the detailed X-ray photoelectron spectroscopy study, only a combined model reflecting both models accounts for true microstructure of SiO_x film. The tendency observed in Fig. 4(b) is explained in terms of the preferential sputtering of Si phase due to higher sputtering yield as compared to SiO_2 phase when considering random mixture model as the microstructure of SiO_x film. The other possibility is due to the enhancement of surface process, which increase the rate of oxygen incorporation. Without assist ion beam irradiation, the growth rate is 0.94 nm/min. However, the growth rate is reduced to 0.27 nm/min with assist ion beam irradiation of 150 eV as evidenced by thickness measurement by low resolution TEM. The model of the preferential sputtering would be more plausible.

After post-deposition annealing, we observe PL emissions for samples in the compositional window of $1.1 \leq x_{\text{app}} \leq 1.4$ as shown in Fig. 5. The size of Si crystallites critically depends on oxygen content in the film and exceeds the size of nanocrystal for having appreciable quantum confinement effect for the films with $x_{\text{app}} < 1.1$. On the other hand, the small

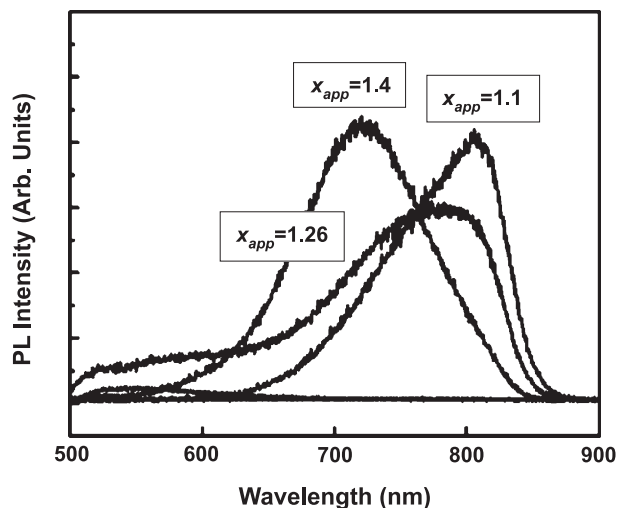


Fig. 5. PL spectra of SiO_x films with various apparent oxygen content, x_{app} after the high temperature N_2 annealing and additional forming gas annealing.

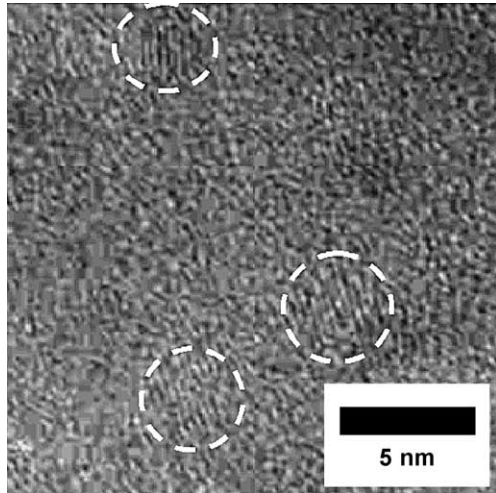


Fig. 6. Cross-sectional TEM image of SiO_{1.26} film containing nanocrystals. White boundaries in the inset are for a guide to an eye.

optical volume of nanocrystals for the films with $x_{app} > 1.4$ is not sufficient for yielding reasonable PL intensity. As observed in Fig. 5, PL show a blue shift as increasing x_{app} . This is due to the stronger quantum confinement effect as decreasing the size of Si nanocrystals. Fig. 6 shows the cross-sectional TEM image of several nanocrystals (~5 nm diameter) in SiO_{1.26} film and supports the idea that observed PL is attributed to Si nanocrystals in the films. The samples grown under ion irradiation shown in Figs. 3 and 4(b) will not exhibit any appreciable PL because $x_{app} > 1.4$. This is confirmed in Fig. 7. SiO_x films under ion beam irradiation show only weak PL band at around 550 nm presumably due to matrix defects similar to the report by Min et al. [18].

The controllability of x in SiO_x films by assist ion beam irradiation can be utilized for area-selective formation of Si nanocrystals. As illustrated in Fig. 1, a shadow mask is inserted in secondary ion beam. The mask is grounded for preventing charging effect. Otherwise, secondary ions would be repelled by Coulomb repulsion. Preliminary experiment employs a mask having three rectangular holes

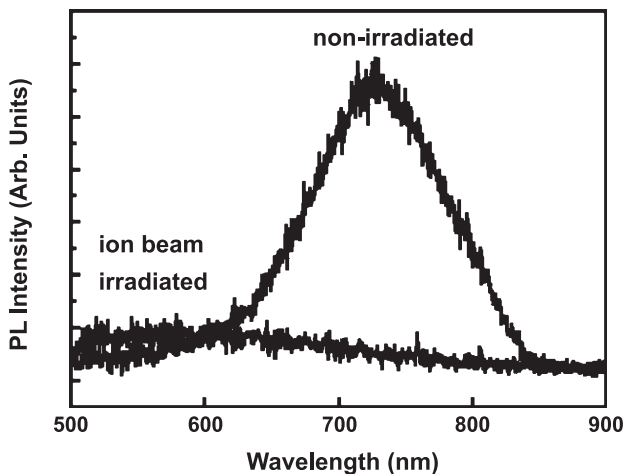


Fig. 7. PL spectra of SiO_x films with and without ion beam irradiation.

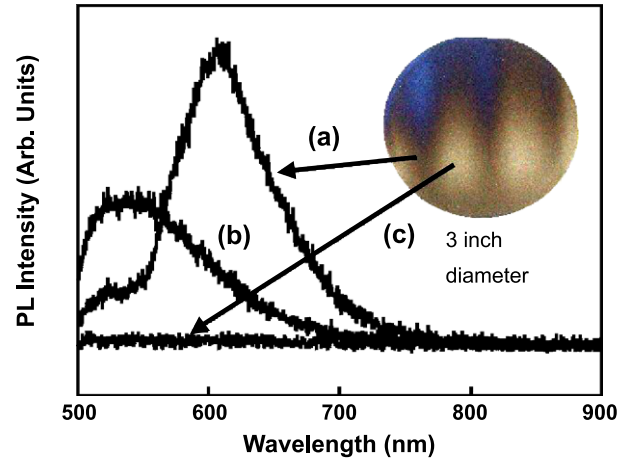


Fig. 8. PL spectra recorded from the different parts of 3-in. sample grown with a shadow mask. O₂ partial pressure is 1.9×10^{-3} Pa during deposition. The photograph shown in the inset is the photograph of 3-in. sample after the deposition. Parts (a) and (c) are non-irradiated and irradiated regions, respectively. Part (b) is the transition region between (a) and (c).

and ion beam with 200 eV ion energy is directed to 3-in. Si wafer through the holes during DIBS. Fig. 8 shows PL spectra recorded from the different parts of 3-in. SiO_x sample after the deposition of SiO_x with the same partial pressure in Fig. 7. The inset in Fig. 8 shows the photograph of 3-in. SiO_x sample. Due to the refractive index alteration by ion beam irradiation, the mask pattern is clearly discernable by the naked eye. However, the pattern is distorted, specifically, the width of non-irradiated region is narrower due to the significant spread of assist ions after escaping from the mask hole. The beam is not neutralized. Therefore, the fact of large spread of irradiated zone might be due to surface charging effect.

The PL spectrum from non-irradiated region shows the maximum intensity at 615 nm and is blue-shifted by 115 nm as compared to PL from the non-irradiated sample shown in Fig. 7. The result indicates that nominally non-irradiated region is actually affected by ion beam irradiation playing a role in the increase of x . The central part of irradiated region show no PL as expected. The transition region between non-irradiated and irradiated regions shows PL centered at 550 nm. The utilization of oxygen ions instead of inert Ar ions for assist ions may results in better area-selectivity. However, the high reactivity of oxygen has led to early failure of tungsten filament of assist ion source. The sustainable time of tungsten filament was usually within an hour and did not allow repeatable investigations.

4. Conclusion

We have investigated the deposition of SiO_x films by DIBS technique. We have shown the advantage of DIBS in preparing SiO_x films with desired oxygen content x by adjusting oxygen partial pressure. We have observed the intense PL from SiO_x samples with oxygen content x in the

narrow range of $1.1 < x_{\text{app}} < 1.4$, after post-deposition annealing at 1100 °C. The formation of Si nanocrystals responsible for PL was confirmed by cross-sectional TEM observation. In addition, we have investigated secondary ion beam irradiation effect during deposition. Secondary ion beam irradiation changes PL peak presumably due to the oxygen content modulation in ion-beam exposed region. The property was utilized for achieving the area-selective formation of Si nanocrystals by inserting a shadow mask in assist ion beam during deposition. Though preliminary results show a spread of ion beam and distortion of exposed pattern, the technique developed here may offer a process advantage during future ULSI processes when optimized.

Acknowledgment

This work was supported by grant no. R05-2002-000065-0 from the Basic Research Program of the Korea Science and Engineering Foundation.

References

- [1] L.T. Canham, Appl. Phys. Lett. 57 (1990) 1046.
- [2] K.S. Min, PhD thesis, Caltech, USA, 2000.
- [3] F. Iacona, G. Franzo, C. Spinella, J. Appl. Phys. 87 (2000) 1295.
- [4] S. Lombardo, S.U. Campisano, Mater. Sci. Eng., R Rep. 17 (1996) 281.
- [5] S. Lombardo, S. Coffa, C. Bongiorno, C. Spinella, E. Castagna, A. Sciuto, C. Gerardi, F. Ferrari, B. Fazio, S. Privitera, Mater. Sci. Eng., B, Solid-State Mater. Adv. Technol. 69–70 (2000) 295.
- [6] H.J. Cheong, J.H. Kang, J.K. Kim, Y. Kim, J.-Y. Yi, T.H. Chung, H.J. Bark, Appl. Phys. Lett. 83 (2003) 2922.
- [7] M. Zacharias, J. Heitmann, R. Scholz, U. Kahler, M. Schmidt, J. Blasing, Appl. Phys. Lett. 80 (2002) 661.
- [8] M. Fujii, S. Hayashi, K. Yamamoto, Jpn. J. Appl. Phys. 30 (1991) 687.
- [9] J.-S. Bae, S.-H. Choi, K.J. Kim, D.W. Moon, J. Korean Phys. Soc. 43 (2003) 557.
- [10] C. Weissmantel, Thin Solid Films 32 (1976) 11.
- [11] J.M.E. Harper, J.J. Cuomo, H.R. Kaufman, J. Vac. Sci. Technol. 21 (1982) 737.
- [12] J.J. Cuomo, S.M. Rossnagel, H.R. Kaufman, Handbook of Ion Beam Processing Technology, Noyes Pub, Park Ridge, 1989.
- [13] M.F. Lambrinos, R. Valizadeh, J.S. Colligon, Nucl. Instrum. Methods Phys. Res., B Beam Interact. Mater. Atoms 127/128 (1997) 369.
- [14] S.K. Ray, S. Das, C.K. Maiti, S.K. Lahiri, N.B. Charkrabarti, Appl. Phys. Lett. 58 (1991) 2476.
- [15] P.G. Pai, S.S. Chao, Y. Takagi, G. Lucovsky, J. Vac. Sci. Technol., A, Vac. Surf. Films 4 (1986) 689.
- [16] H.R. Philipp, J. Non-Cryst. Solids 8–10 (1972) 627.
- [17] R.J. Temkin, J. Non-Cryst. Solids 17 (1975) 215.
- [18] K.S. Min, K.V. Shcheglov, C.M. Yang, H. Atwater, M.L. Brongersma, A. Polman, Appl. Phys. Lett. 69 (1996) 2033.